Focusing through dynamic tissue with millisecond digital optical phase conjugation

Daifa Wang,[1,2,†] Edward Haojiang Zhou,[1,†] Joshua Brake,[1] Haowen Ruan,[1] Mooseok Jang,[1] and Changhuei Yang[1,*]

[1]Departments of Electrical Engineering and Bioengineering, California Institute of Technology, Pasadena, California 91125, USA
[2]Key Laboratory for Biomechanics and Mechanobiology of Ministry of Education, School of Biological Science and Medical Engineering, Beihang University, Beijing, China
*Corresponding author: chyang@caltech.edu

Digital optical phase conjugation (DOPC) is a new technique employed in wavefront shaping and phase conjugation for focusing light through or within scattering media such as biological tissues. DOPC is particularly attractive as it intrinsically achieves a high fluence reflectivity in comparison to nonlinear optical approaches. However, the slow refresh rate of liquid crystal spatial light modulators and limitations imposed by computer data transfer speeds have thus far made it difficult for DOPC to achieve a playback latency of shorter than ~200 ms and, therefore, prevented DOPC from being practically applied to thick living samples. In this paper, we report a novel DOPC system that is capable of 5.3 ms playback latency. This speed improvement of almost 2 orders of magnitude is achieved by using a digital micromirror device, field programmable gate array (FPGA) processing, and a single-shot binary phase retrieval technique. With this system, we are able to focus through 2.3 mm living mouse skin with blood flowing through it (decorrelation time ~30 ms) and demonstrate that the focus can be maintained indefinitely—an important technological milestone that has not been previously reported, to the best of our knowledge.   © 2015 Optical Society of America

OCIS codes: (110.0113) Imaging through turbid media; (070.5040) Phase conjugation; (110.0180) Microscopy.

http://dx.doi.org/10.1364/OPTICA.2.000728

1. INTRODUCTION

Focusing light through tissues has long been a challenge for biomedical optics. The turbid nature of tissues strongly scatters light and hinders the formation of a sharp focus. Recently, research in the field of wavefront shaping has shown that by correcting the wavefront incident on scattering media, focus can be constructed at an arbitrary location behind the sample [1,2]. Different strategies have been developed to realize this process including iterative wavefront optimization [1,3–5], transmission matrix measurement [6–8], and optical phase conjugation (OPC) [9–11]. Among these, OPC implements the corrected wavefront by recording the scattered light field globally and then playing back the conjugate light field by a phase conjugate mirror (PCM) without time-consuming iterations. Since the process of elastic light scattering is time symmetric, by playing a conjugate version of the scattered wavefront back through the scattering medium, the conjugate input wavefront can be recovered.

By employing OPC, a number of novel techniques for focusing light through or within a scattering medium have recently been developed. These include time-reversed ultrasonically encoded light (TRUE) [12,13], time reversal of variance-encoded light (TROVE) [14], time reversal by analysis of changing wavefronts from kinetic targets (TRACK) [15], and time-reversed adapted-perturbation (TRAP) focusing [16]. These methods have

the potential to improve or enable biomedical applications such as deep tissue imaging, photodynamic therapy, and noninvasive cytometry.

There are two major advantages of OPC compared to other wavefront shaping techniques. First, it is able to arrive at the correct wavefront solution without iteration. Second, the number of controllable optical modes in the playback wavefront can be very high, $\sim 5 \times 10^5$ modes or more. Optical phase conjugation methods can be categorized into two primary groups. Nonlinear OPC methods [12,17,18] employ nonlinear crystals to store the scattered field and propagate the phase conjugate field. In contrast, the digital optical phase conjugation (DOPC) method [13–16] uses an electronic camera in an interferometric setup to capture the optical wavefront information and subsequently produce a suitable OPC field by using that information to pattern a spatial light modulator (SLM).

The DOPC method has several intrinsic advantages over nonlinear OPC methods. First, whereas nonlinear crystals are strongly dependent on wavelength, DOPC can freely work with a broad range of wavelengths. Second, DOPC provides the flexibility to render wavefront playback beyond a single OPC field. In fact, TROVE, TRACK, and TRAP all exploit this unique capability of DOPC to render complex and nuanced wavefronts. In the case of TRACK and TRAP, for example, the rendered wavefront is

actually a differential DOPC wavefront. Third, and perhaps most important, the DOPC method has the intrinsic ability to achieve a fluence reflectivity greater than unity. Here, we define fluence reflectivity as the ratio between the total amount of light that one can play back on the conjugate wavefront to the total amount of scattered light required to determine the conjugate wavefront in the first place. While nonlinear OPC methods can in principle provide gain enhancement by temporally squeezing the playback photon packet [19], a practical and useful approach to deliver large amounts of energy over an extended period of time has not been demonstrated.

Currently, the DOPC method does have a significant disadvantage versus nonlinear OPC methods' response speeds. Recently, nonlinear methods with system response latencies of the order of milliseconds have been reported [20,21]. In contrast, DOPC systems reported thus far have response times of the order of hundreds of milliseconds or more [22]. This slow response is due to the use of slow liquid crystal SLMs and conventional personal computer (PC)-based data transfer. Fast response speed is a key criterion if we are to apply OPC methods usefully for *in vivo* applications in thick samples. This is mainly due to the dynamic nature of biological tissue caused by the constant motion of the scatterers within. This rate of change is dependent both on sample thickness and the degree of immobilization. As a reference point, the scattered field of 532 nm light through an unclamped living mouse skin flap has a speckle decorrelation time of ~30 ms. When the same tissue is clamped, this decorrelation time increases to ~300 ms [22].

The primary goal of this paper is to show that the use of a high-speed digital mirror device (DMD) and field programmable gate array (FPGA) data processing allows DOPC to achieve high response speeds, as well. While using the binary modulation of the DMD to accomplish wavefront shaping may seem

counterintuitive, and the oblique reflection angle significantly complicates DOPC system alignment, overcoming these challenges enables us to incorporate the strengths of the DOPC while minimizing the response time of the system. In this paper, we report a novel DMD-based DOPC system with a demonstrated playback latency of 5.3 ms. We demonstrate that our system is capable of focusing light through 2.3 mm thick unclamped mouse dorsal skin with a decorrelation time of less than 30 ms. By repeating the DOPC procedure 50 or even more times per second, we are able to maintain indefinitely the focus through the living sample. This demonstration of sustainable focusing through a thick living sample with blood flowing through it is the first of its kind and opens the door for new applications of OPC in the deep tissue regime of live biological samples.

2. METHODS

A simplified schematic of the DMD-based DOPC system is shown in Fig. 1(a). A complete optical scheme can be found in Supplement 1. The light paths of the setup for recording and playback are shown in Figs. 1(b) and 1(c), respectively. As shown in Fig. 1(b), in the recording step, all the pixels on the DMD are turned off. This causes the playback beam to diffract away from Camera 1 and onto a beam dump. The sample beam and reference beams are combined at BS3, reflected by BS4 and Mirror 2, and travel back through BS4 to Camera 1, where their interference pattern is measured. In the playback step shown in Fig. 1(c), the FPGA processes the camera data to generate a suitable wavefront solution and sends it to the DMD, which displays the corresponding phase map. The playback beam then propagates through BS4, BS3, and L3 to the sample. Meanwhile, the sample beam is blocked by a fast shutter to prevent backscattering off the sample. This playback process results in a focus
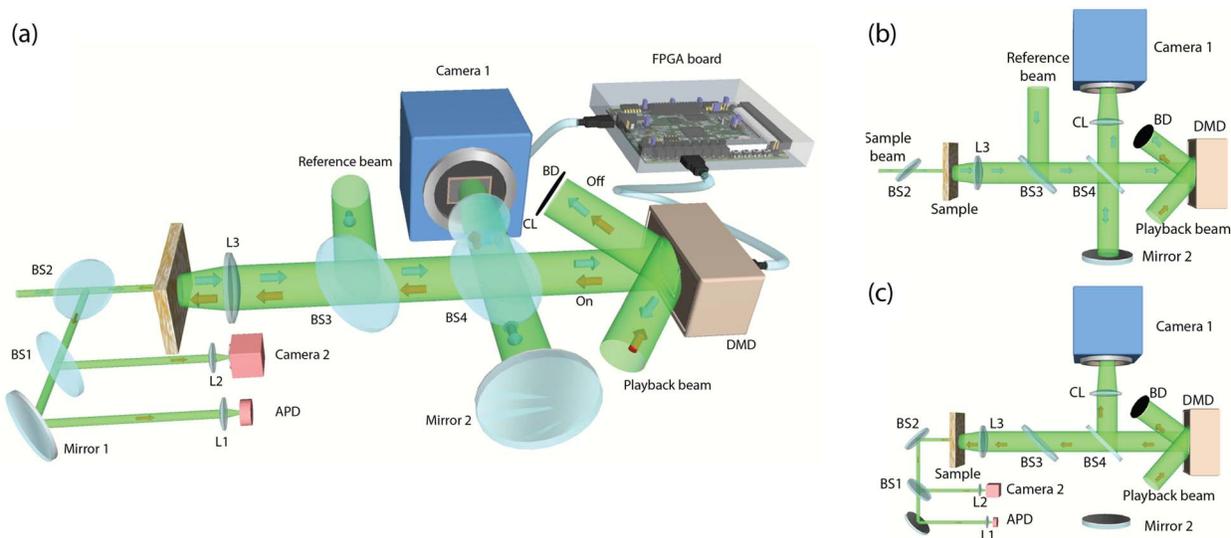

Fig. 1. (a) Simplified schematic of the DMD-based DOPC. A 2.5 mm diameter collimated beam from the laser source (Excelsior 532 nm single mode, 200 mW, Spectra-Physics) is incident onto the sample through BS2. Scattered light from the sample is collected by L3 and is combined with the reference beam by BS3. The combined reference and sample beam is reflected by BS4 and Mirror 2, passes through BS4, and is captured by Camera 1 (pco.edge 5.5, PCO-TECH). The DMD (W4100, Wintech) and Mirror 2 are aligned symmetrically with reference to BS4, and the DMD surface is imaged onto the camera sensor chip by CL (AF-S VR Micro-NIKKOR 105 mm f/2.8G IF-ED, Nikon) with pixel-to-pixel alignment. Camera 1 and the DMD are connected through a host FPGA (ViClaro IV GX Camera Link Development Kit, Microtronix). The conjugate result is observed on Camera 2 (Prosilica GX 1920, Allied Vision) and the APD (SPCM-AQRH-14, Excelitas). (b) Optical path schematic of the recording step. (c) Optical path schematic of the playback step (L, lens; BS, beam splitter; BD, beam dump; CL, camera lens; APD, avalanche photodiode).

observed through the sample on Camera 2 and a corresponding peak recorded by the avalanche photodiode (APD). As the reference beam and playback beam are two separate beams, the fluence reflectivity is limited only by the damage threshold of the DMD and the laser power. In our system, the fluence reflectivity was set at 2000. As response speed is a design priority, each major component of this system is chosen and adapted for this purpose. We will discuss each component in the following subsections.

A. Single-Shot Binary Phase Retrieval

To compute the correct phase map to display on the DMD, Camera 1 captures the interference pattern between the reference field $E_{ref}(x, y)$ and the sample field $E_{sam}(x, y)$. This interference pattern can be described as: $I_i(x, y) = I_{ref}(x, y) + I_{sam}(x, y) + 2\sqrt{I_{ref}(x, y)I_{sam}(x, y)} \cos|\Delta\theta|$, where $I_{ref}(x, y)$ and $I_{sam}(x, y)$ are the intensity of the reference and sample fields, respectively, and $\Delta\theta$ is their phase difference. By setting $\langle I_{sam}(x, y)\rangle \ll I_{ref}(x, y)$, $I_i(x, y)$ can be approximated as

$$I_i(x, y) \approx I_{ref}(x, y) + 2\sqrt{I_{ref}(x, y)I_{sam}(x, y)} \cos|\Delta\theta|. \quad (1)$$

Then, $I_{ref}(x, y)$ can be measured independently by blocking the sample beam and, by comparing it to $I_i(x, y)$, we can determine the range in which the absolute phase difference $|\Delta\theta|$ lies

$$I_i(x, y) < I_{ref} \rightarrow \frac{\pi}{2} < |\Delta\theta| \leq \pi,$$

$$I_i(x, y) > I_{ref} \rightarrow 0 \leq |\Delta\theta| \leq \frac{\pi}{2}. \quad (2)$$

In this way, the intensity of the interference pattern at a point (x, y) can be used to recover the binary phase of $E_{sam}(x, y)$ in a single shot. In comparison, two methods commonly applied in DOPC systems, phase stepping holography [23] and off-axis holography [24], are capable of fully recovering the sample field but sacrifice either speed or spatial resolution. While DOPC playback with binary phase information is less efficient than with perfect phase information, this small sacrifice in efficiency yields a large enhancement in response speed.

B. FPGA-Based Data Processing and Transfer

An FPGA board [as shown in Fig. (2)] is implemented in the DOPC system for data processing and transfer. It has a camera link connection directly to the recording camera and a high definition multimedia interface (HDMI) connection to the DMD. This allows full frame (1920 × 1080) interference pattern transfer in 5.0 ms (6.8 Gb/s) and full frame size phase map transfer in 1.56 ms (1.8 Gb/s). Here, the phase map transfer time is the time from starting the binary phase data transfer to completing the stable display on the DMD. Although the DMD chip (DLP9500, TI) has a fast refreshing speed of up to 23 K fps, the standard 60 Hz HDMI display interface of the W4100 board limits the performance. To fully utilize the fast response speed of the DMD, we designed custom firmware for the FPGA controller (Virtex 5, Xilinx) on the W4100 board. With a custom HDMI protocol, we encode 24 binary pixels into one 24 bit RGB pixel of standard HDMI, allowing us to achieve fast binary image transfer. In the recording step, the FPGA board reads out the interference image from the recording camera and retrieves the phase in parallel. Once the phase map is ready and has been adjusted to compensate for the curvature of the DMD (see Supplement 1), it is transferred to the DMD board and displayed. Compared to a computer, the FPGA allows for greatly accelerated data processing
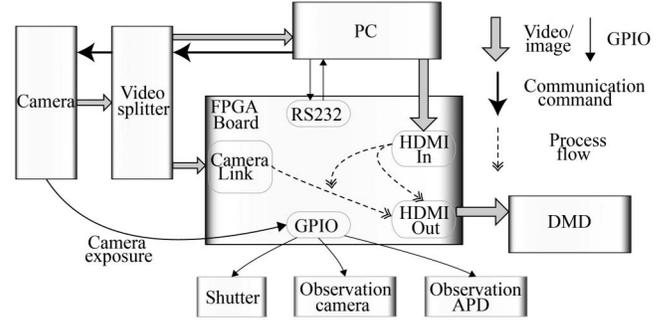

Fig. 2. Functional schematic of the FPGA-based DOPC.

and transfer speeds. When using a PC as the host processor in DOPC, the multitask scheduling and hardware access wrapping in modern operating systems limits the latency between recording and playback steps to a minimum of around 200 ms [22]. In contrast, as an FPGA inherently has a highly parallel computing capacity, the processing latency for binary phase retrieval is eliminated by overlapping the phase processing with the camera image transfer. In addition to the speed of the FPGA system, our setup allows for data collection and processing to be seamlessly switched to the PC for time-insensitive optical system debugging and pixel–pixel alignment between the recording camera and the DMD. To achieve this, a video splitter (CLV-402, Vivid Engineering) is implemented to switch the output of the recording camera between the PC and the FPGA. An HDMI interface is also set up between the PC and FPGA to allow the PC to transfer phase maps to the DMD.

C. DMD-based Phase Conjugation

When a conjugate phase map is displayed on the DMD, the DMD implements a binary amplitude modulation scheme [25] to construct a conjugate focus through the tissue. Here we will analyze the binary phase modulation scheme, which, although essentially identical to binary amplitude modulation, is formulated here to easily integrate into the framework of phase conjugation [26].

When using the DMD for light modulation, every individual micromirror acts as a diffractive element and together the whole DMD acts as a 2D blazed grating. As shown in Fig. 3(a), when a pixel is turned on, it will tilt 12° clockwise in the diagonal direction. This oblique angle complicates the DOPC system design, as it is a challenge that does not exist for SLM-based DOPC systems. To address this, we choose to illuminate the DMD with an appropriately tilted light field such that the diffracted light propagates perpendicularly with respect to the surface of the DMD. This propagation direction is subject to the blazed grating equation, which is a function of the center-to-center distance between the individual micromirrors in the array (d), the angle of incidence (ϕ) with respect to the DMD surface normal, the wavelength (λ), and the diffraction order (n). Setting the diffraction angle to fix the diffraction direction normal to the DMD surface yields a simplified form of the blazed grating equation

$$d \sin\phi = n\lambda. \quad (3)$$

However, in order to achieve the maximum possible intensity of the diffraction beam, the incident angle should be chosen so that the central peak of the $sinc^2$ envelope determined by the
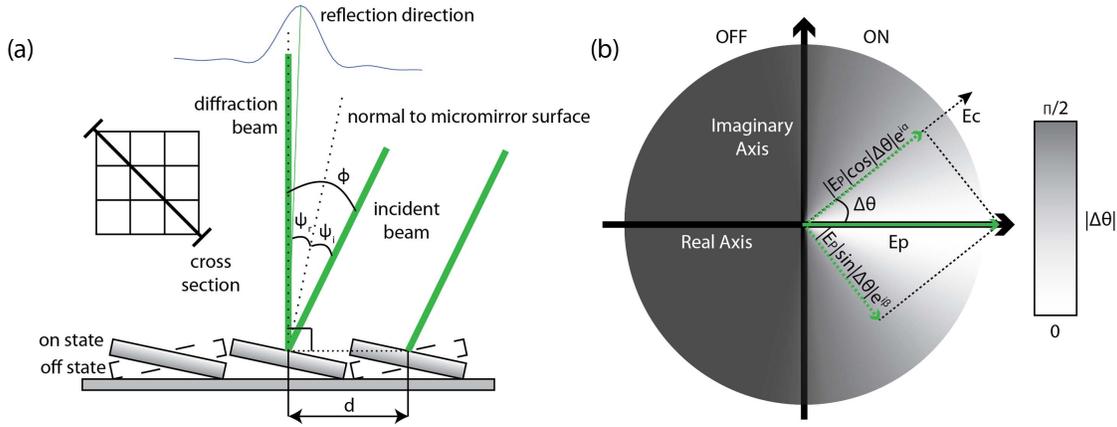
Fig. 3. (a) DMD diffraction demonstration. (b) Binary phase modulation of a DMD. E_p is the field played back by the DMD, E_c is the desired phase conjugate field, and $\Delta\theta$ is the phase difference between E_c and E_p. When a pixel of the DMD is turned on, it plays back the phasor E_p, which can be decomposed into two orthogonal components. One is in the direction of the desired phase conjugate field E_c with an amplitude modulated by $\cos|\Delta\theta|$ and contributes to the focus. The other component orthogonal to E_c is modulated by $\sin|\Delta\theta|$ and contributes to the background.

direction of the specular reflection from each individual micro-mirror matches as closely with the direction normal to the DMD surface as possible. Combining the simplified blazed grating equation above with the law of reflection ($\psi_i = \psi_r$), which determines the location of the sinc^2 envelope, we can solve for the incident angle to maximize the intensity of the diffracted beam. Given a light source with a wavelength of 532 nm and $d = 10.8\sqrt{2}$ μm from the dimensions of the DMD, we solve to find the optimum incident angle and diffraction order to be $\phi = 24.7°$ and $n = 12$, respectively.

After optimizing the alignment of the DMD in the DOPC system, we fit the binary amplitude modulation of the DMD into a phase conjugation framework. Since the diffracted light from the DMD has a uniform phase, we can spatially choose whether it is played back or not by manipulating each pixel's state. As shown in Fig. 3(b), without loss of generality, we suppose playback beam E_p has uniform amplitude A and phase zero. For an electric field $E_c = |E_c|e^{i\alpha}$, which is the optimal phase conjugate solution to be played back, there is a phase difference $\Delta\theta$ between E_c and E_p. Using the binary phase retrieval algorithm described earlier, we determine whether an individual pixel should be played back. If $|\Delta\theta|$ is less than $\pi/2$, the corresponding pixel is turned on. Otherwise, it is turned off. When we turn on the pixel, E_p can be decomposed into orthogonal phase vectors, as shown in Fig. 3(b). This allows us to derive the phase modulation function of the DMD in DOPC as

$$f(|\Delta\theta|) = \begin{cases} 0, & \frac{\pi}{2} < |\Delta\theta| \leq \pi \\ \cos|\Delta\theta|e^{i\alpha} + \sin|\Delta\theta|e^{i\beta}, & 0 \leq |\Delta\theta| \leq \frac{\pi}{2} \end{cases}. \quad (4)$$

This means that when $0 \leq |\Delta\theta| \leq \frac{\pi}{2}$ and a pixel of the DMD is turned on to represent a certain E_c, we will play back the electric field $|E_p|\cos|\Delta\theta|e^{i\alpha}$, which has the phase of E_c and amplitude modulated by $\cos|\Delta\theta|$, along with an orthogonal electric field $|E_p|\sin|\Delta\theta|e^{i\beta}$ with amplitude modulated by $\sin|\Delta\theta|$. The cosine term will be played back as a correct component of the phase conjugate field, and construct a peak. The sine term, which has an orthogonal phase, will make no contribution to the peak recovery and will form a background in the playback field. Following a similar derivation in Refs. [13,25] (see details in Supplement 1),

we find the theoretical peak-to-background ratio (PBR) for DMD-based DOPC to be

$$\text{PBR} = \frac{1/2 + (N-1)/2\pi}{M} \approx \frac{N}{2\pi M}, \quad (5)$$

where M is the number of modes in the focus, and N is the number of controllable modes on the DMD. Implementing the DMD in the DOPC setup allows our system to save more than 10 ms for conjugate phase display compared to the time reported in liquid-crystal (LC)-SLM-based DOPC systems [13,15,22]. When a voltage is applied to an LC-SLM based on nematic liquid crystal technology, it usually takes over 10 ms to turn to the specified direction. This limits the refresh rate to tens of hertz. In contrast, a DMD, which is based on microelectromechanical system (MEMS) technology, has a response time of around 18 μs with a 23 kHz refresh rate [27], over 2 orders of magnitude faster than typical LC-SLMs.

D. Workflow of Fast DOPC

The workflow of our system is shown in Fig. 4. Prior to operation, the reference beam intensity distribution is recorded. Then the DOPC loop starts. At the beginning of every loop, all of the DMD pixels are turned off and the interference pattern is captured. Once the intensity of a pixel is transferred from the camera and stored by the FPGA, its binary phase is processed and recovered. After all the pixels are processed, the binary phase map is transferred to the DMD and displayed for a designated time. During the process, the fast shutter, exposure of the observation camera, and the recording of the APD signal are synchronized by the FPGA general purpose input/outputs (GPIOs). Each loop is synchronized by the exposure and transfer signals of the recording camera.

As shown in Fig. 4, the playback latency is the sum of the time required by the recording exposure, data transfer from the recording camera to the FPGA (recording transfer), and binary phase transfer from the FPGA to the DMD (phase transfer). For a full frame size of 1920 × 1080 (up to $2.1 × 10^6$ controllable modes) and 0.5 ms exposure, the time from the start of the exposure to playback is 7.06 ms. A rolling shutter is used for the recording exposure, so neighbor rows start to expose successively with a 9.17 μs delay. The time latency is calculated from the average
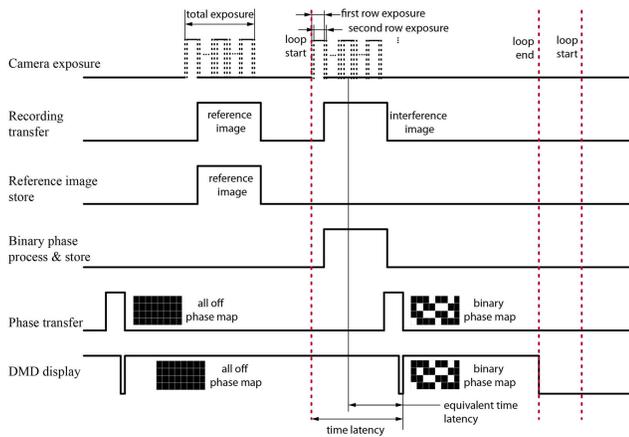
Fig. 4. Workflow of the FPGA-based DOPC.

exposure start time to the time playback starts. The latency is quantified by the following experiments.

3. RESULTS

A. Playback Latency Quantification

To evaluate the actual playback latency of our system, DOPC experiments were conducted on tissue samples with a controllable decorrelation time using a moving tissue strategy [20]. A piece of 3 mm thick chicken breast ($\mu_s = 30/\text{mm}$, $g = 0.965$) was sandwiched between two 1 mm thick glass slides. In the middle layer, a 3 mm thick U-shaped spacer was placed surrounding the chicken

breast to guarantee its thickness and mobility [as shown in Fig. 5 (a)]. During the experiment, samples were changed before they dried out to ensure their scattering properties. The whole sample was held by a translation stage with a motorized actuator (LTA-HS, Newport) to generate different decorrelation times by varying the lateral velocity.

The decorrelation time of the tissue itself was several seconds [13], which meant that the amount of decorrelation in a period of several milliseconds was negligible. To avoid the effects of slow decorrelation when the stage was accelerating, experiments were done when the stage had reached full speed. Tissue decorrelation curves when lateral velocity was set to 0.2 mm/s and 0.25 mm/s are shown in Figs. 5(b) and 5(c), respectively. Here we define the decorrelation time τ as the time t when the speckle correlation coefficient r_c decreases to $1/e$. Fitting with a Gaussian function $r_c = e^{-t^2/\tau^2}$ [28], we can find the decorrelation time τ is 6.2 and 5.0 ms for each case. The conjugate focus results for the two cases are shown in Fig. 5(d). Given that the motion-induced degradation ratio of PBR is identical to the drop in the speckle correlation coefficient [22], it is straightforward to conclude that the system playback latency is identical to the decorrelation time of the sample when the PBR achieved on a moving sample is $1/e$ of the static PBR. From the results, the PBR is 88 for 0.2 mm/s and 56 for 0.25 mm/s. Comparing these to the value of the static PBR divided by e (~65), we can tell the time latency is slightly more than 5.0 ms, which can be accurately calculated as 5.3 ms.

B. OPC Efficiency Quantification

As shown in Eq. (5), PBR is related to both number of input modes (N, number of speckle grains on the DMD) and number
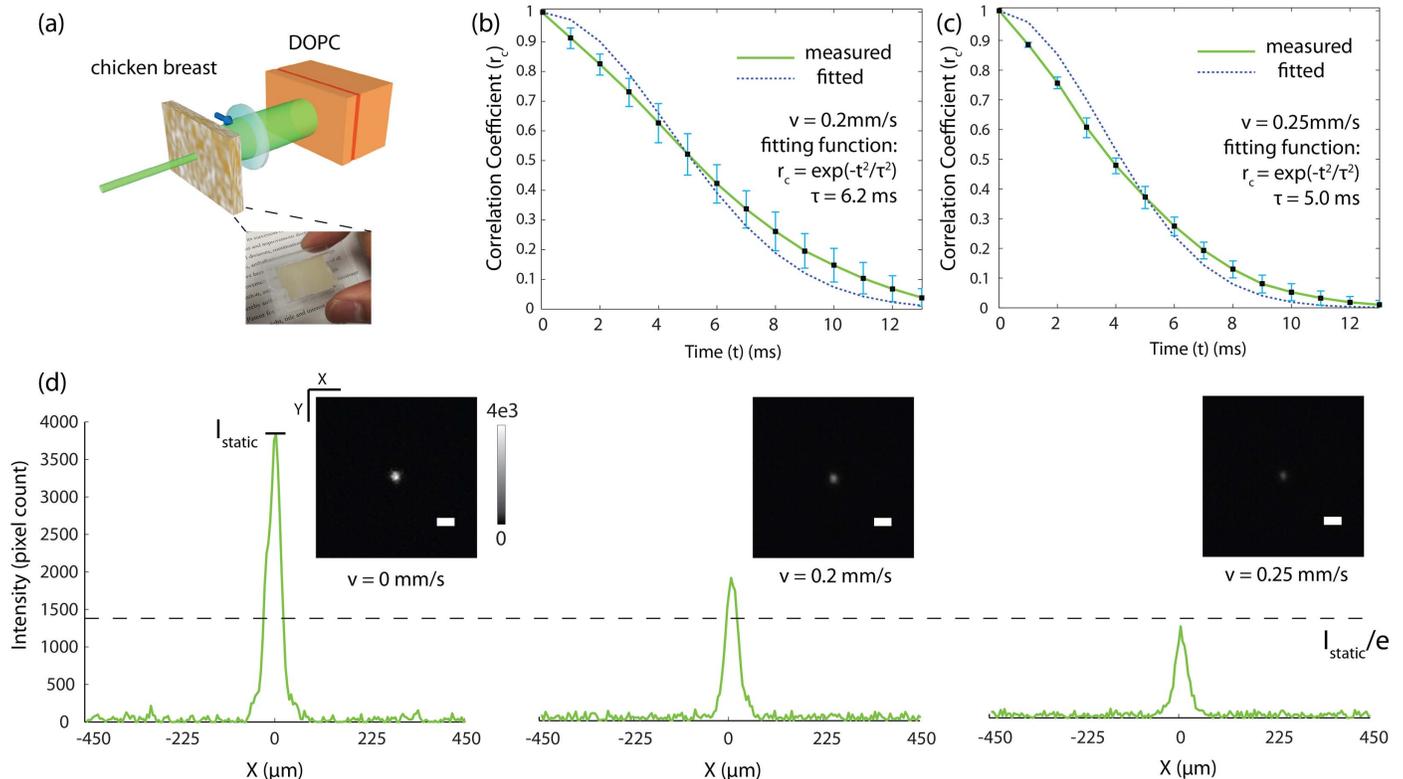

Fig. 5. (a) Moving sample setup. (b),(c) Moving sample speckle decorrelation curves at lateral velocity 0.2 and 0.25 mm/s. Error bars indicate standard deviation over 10 datasets. (d) Conjugate focus images and cross-section peak plots when the sample was static, moving at 0.2 and 0.25 mm/s.

of output modes (M, number of speckle grains in the focus). Therefore, it is not a fair comparison to quantify DOPC performance merely by the PBR for different numbers of output modes. However, OPC efficiency, which is the ratio of PBR achieved on a system to theoretical PBR, sets a suitable standard for different systems. To evaluate the OPC efficiency of our system, we used our DOPC system to focus light through an opal diffuser (10DIFF-VIS, Newport). Based on the derivation of DMD-based conjugation and the measured interference pattern on the recording camera, we determined the speckle size to be 4 pixels wide on the DMD. Since the DMD has 1920×1080 pixels, the number of optical modes we can access with the DMD equals 1.3×10^5. To determine the number of modes in the focus, we examined the conjugate focus through the sample. When the conjugate beam was played back, we observed a focus on the observation camera with a PBR of 630 and full width at half-maximum (FWHM) of 45 µm, as shown in Fig. 6. When we displayed a random pattern on the DMD, the speckle FWHM was 13 µm, computed from the autocorrelation of the speckle pattern. From these two measurements, we can find that the number of modes in the focus is ~12. From the PBR equation, we calculated the optimal PBR as $1.3 \times 10^5/(12 \cdot 2\pi) \approx 1700$, which means our system performance has an efficiency of 37%.
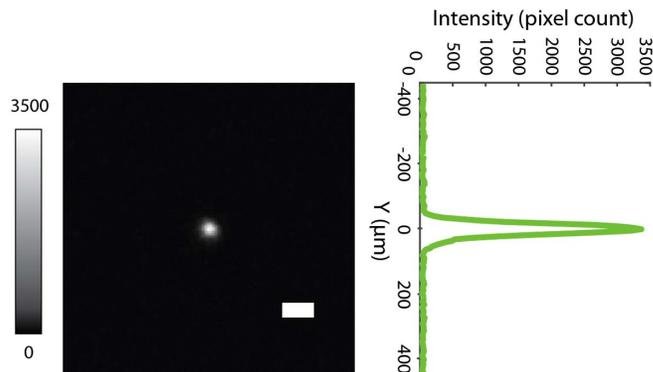

Fig. 6. PBR quantification. Scale bar is 100 µm.

C. *In Vivo* Experiments

In vivo experiments were demonstrated by focusing through the dorsal skin of a living mouse. For the *in vivo* sample, a regular white laboratory mouse was shaved on the dorsal skin flap. Then its dorsal skin was mounted to a clip device. Isoflurane was implemented as the inhalational anesthesia both in preparation and during the experiment. All of these procedures and the dosage of chemicals followed protocols of the Institutional Animal
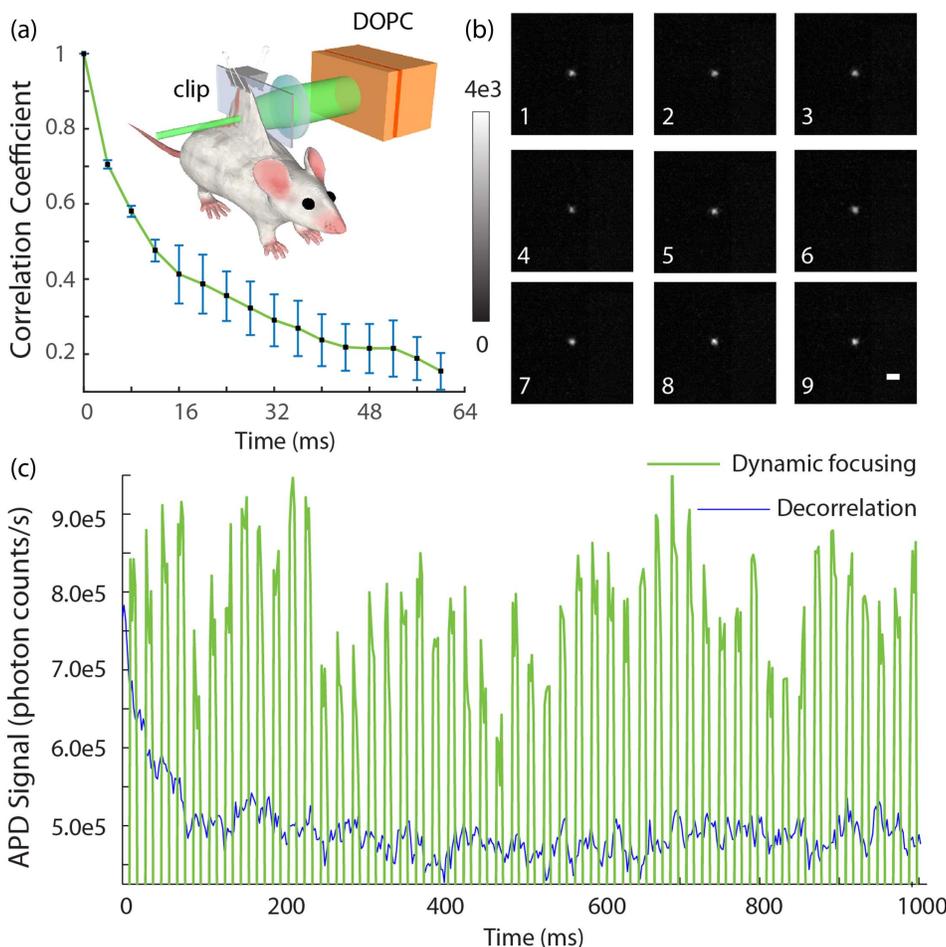

Fig. 7. (a) Clipped mouse dorsal skin setup and speckle decorrelation curve of *in vivo* tissue. Error bars indicate standard deviation over 10 datasets. (b) Continuous conjugate foci through clipped sample (see also Visualization 1). (c) APD plot for sustainable foci and decorrelation focus. Scale bar is 100 µm. In the experiment, to accurately distinguish the focus intensity from background in the APD signal, a background (I_b) was measured first when the focus totally vanished, which is 5×10^5 in the APD plot.

Care and Use Committee at the California Institute of Technology.

As shown in Fig. 7(a), a clip fixed the upper edge of the skin on a transparent plastic plate, which was placed at the sample position. In this way, the bottom of the dorsal skin was in a natural free status. The sample beam was incident onto the bottom part of the skin, which had a thickness of around 2.3 mm. Before DOPC was applied, a series of scattering speckle patterns from the tissue were captured by the recording camera to analyze the tissue decorrelation time and form the decorrelation curve plotted in Fig. 7(a). From this curve we can tell its decorrelation time is 28 ms, where the decorrelation time is defined as the time when the speckle correlation coefficient decreases to $1/e$. After that, DOPC was conducted with an exposure time of 0.5 ms on the recording camera, at a refresh rate of 50 Hz and a playback holding time of 10 ms. A series of images from the observation camera triggered by the playback signal with an exposure time of 3 ms are included in Fig. 7(b) and Visualization 1 (5 s video) along with a corresponding APD plot in Fig. 7(c). From the focus images and APD plot, we can tell a clear focus was constructed and maintained through unrestricted tissue on a living animal. From the average of 10 images, we calculate that the PBR is 180. For our system, a refresh rate up to 100 Hz with flexible holding time is achievable. It should also be noted that in the middle of the movie we can observe a short failing of conjugation due to severe body movement from respiration, not due to the decorrelation of the tissue itself.

4. DISCUSSION AND CONCLUSION

In this work, we demonstrated what we believe to be the first DMD-based DOPC system. This system is capable of playback with latency of the order of milliseconds, a speed improvement of approximately 2 orders of magnitude over prior DOPC systems. Using the fast DOPC system, we demonstrated the ability to create an indefinitely sustainable focus through unrestricted tissue on a living animal, a capability that has not been previously reported for any OPC experiments. While nonlinear approaches can, in principle, provide this capability as well, this DOPC approach is direct and can provide a greater than unity fluence reflectivity. Our system can achieve greater than 2000 fluence reflectivity, which is crucial for thick *in vivo* tissue application. In our case, the playback beam is set to ~10 mW and the total fluence of the scattered light from the sample is ~5 μW. We further quantified our playback latency as 5.3 ms. While the background due to unmodulated light will need to be addressed in the binary phase retrieval method, it will be straightforward to extend this technology to existing OPC-based technology, such as TRUE, TROVE, and TRACK, and apply it in living tissue for biological applications. Compared to phase-only OPC, DMD-based DOPC encounters a PBR reduction of 80% (from $\pi/4$ to $1/2\pi$). However, for the DMD-based DOPC system, the PBR can be further improved by tuning $I_{\text{ref}}/\langle I_{\text{sam}} \rangle$ in the single-shot binary phase retrieval. For example, suppose I_{ref} and I_{sam} have intensities of the same order of magnitude; then the binary phase retrieval equation will be

$$\text{DMD}(x, y) = \begin{cases} 1, & I_i(x, y) < I_{\text{ref}}(x, y) \to |\alpha - \pi| < \phi \\ & \phi = \arccos\left(1/2\sqrt{I_{\text{ref}}/I_{\text{sam}}}\right) < \frac{\pi}{2}. \quad \textbf{(6)} \\ 0, & \text{else} \end{cases}$$

As I_{sam} follows a Rayleigh distribution [29], by comparing the intensity difference we can statistically select a smaller phase range 2ϕ than π. The theoretical PBR in this condition (detailed derivation in Supplement 1) is a unimodal function of $I_{\text{ref}}/\langle I_{\text{sam}} \rangle$, which achieves up to 12.6% higher PBR at $I_{\text{ref}}/\langle I_{\text{sam}} \rangle = 1.61$ than when $I_{\text{ref}} \gg \langle I_{\text{sam}} \rangle$. In our experiments, we selected this condition as closely as possible. However, due to the dynamic and heterogeneous nature of biological tissue, it is likely that the PBR could have been further improved by fine-tuning this ratio to more accurately select this optimal condition.

Recently, focusing through thin *ex vivo* tissue samples (200 μm chicken breast) was demonstrated at submicrosecond timescales by using the self-organization of an optical field inside a multimode laser cavity [30]. Despite its speed, the approach demonstrated only around 1000 controllable modes, and the number of controllable modes will significantly diminish for thicker samples. This hinders its applications to thick *in vivo* tissue. In addition, the technique relies on optical feedback from the target position, preventing it from being extended to noninvasive techniques with a guide star to focus inside biological tissue.

The flexibility of the DOPC system also provides the additional ability to trade-off controllable modes for reduced playback latency. Since the time for recording and phase transfer is proportional to frame size, shrinking the frame size can further decrease the playback latency. For example, if the frame size is reduced to 1920×70, the playback latency is below 1 ms. Although the PBR will also decrease for smaller frame sizes, up to 1.3×10^5 controllable pixels are still available at a frame size of 1920×70. In practice, we could balance the number of controllable modes (PBR) and time latency based on the decorrelation properties of different samples.

The architecture of our DOPC system also has the potential to be applied in microsecond scale wavefront shaping. Currently, the playback latency is determined by the sum of the time required by the recording exposure, data transfer from the camera to the FPGA, and binary phase transfer from the FPGA to the DMD. As the development of fast and sensitive scientific cameras continues, the exposure time and recording transfer time can be reduced by orders of magnitude. Here we have used an exposure time of 0.5 ms, the minimum exposure time available for the camera, which may be reduced to tens of microseconds or even several microseconds in the future. Meanwhile, the sample beam intensity has to match the shorter exposure. This will be hindered by tissue absorption, which can be addressed by switching from the 532 nm laser source to near-infrared wavelengths, which have orders of magnitude lower tissue absorption. The minimal wavelength dependency of the DOPC system compared to nonlinear OPC systems allows this conversion to a different wavelength regime to be direct. We anticipate that with near-infrared light, *in vivo* DOPC applications on tissue centimeters thick can be realized. Finally, a phase transfer time of around 50 μs can be realized by using a better FPGA (e.g., Altera Stratix V) and a custom-designed data transfer interface to match the maximum refresh rate of the DMD (23 kHz). With the development of faster DMD devices, this time may be further reduced to several microseconds. As the decorrelation rate of tissue drastically increases with thickness, such improvements would ultimately enable wavefront shaping to be applied for optogenetics in the whole brain, *in vivo* deep tissue imaging, and photodynamic therapy for internal organs.

See Supplement 1 for supporting content.

REFERENCES

1. I. M. Vellekoop and A. P. Mosk, "Focusing coherent light through opaque strongly scattering media," Opt. Lett. **32**, 2309–2311 (2007).
2. A. P. Mosk, A. Lagendijk, G. Lerosey, and M. Fink, "Controlling waves in space and time for imaging and focusing in complex media," Nat. Photonics **6**, 283–292 (2012).
3. I. M. Vellekoop, A. Lagendijk, and A. P. Mosk, "Exploiting disorder for perfect focusing," Nat. Photonics **4**, 320–322 (2010).
4. D. B. Conkey, A. M. Caravaca-Aguirre, and R. Piestun, "High-speed scattering medium characterization with application to focusing light through turbid media," Opt. Express **20**, 1733–1740 (2012).
5. H. Yilmaz, W. L. Vos, and A. P. Mosk, "Optimal control of light propagation through multiple-scattering media in the presence of noise," Biomed. Opt. Express **4**, 1759–1768 (2013).
6. S. Popoff, G. Lerosey, M. Fink, A. C. Boccara, and S. Gigan, "Image transmission through an opaque material," Nat. Commun. **1**, 81 (2010).
7. T. Chaigne, O. Katz, A. C. Boccara, M. Fink, E. Bossy, and S. Gigan, "Controlling light in scattering media noninvasively using the photo-acoustic transmission matrix," Nat. Photonics **8**, 58–64 (2014).
8. J. Yoon, K. Lee, J. Park, and Y. Park, "Measuring optical transmission matrices by wavefront shaping," Opt. Express **23**, 10158–10167 (2015).
9. Z. Yaqoob, D. Psaltis, M. S. Feld, and C. Yang, "Optical phase conjugation for turbidity suppression in biological samples," Nat. Photonics **2**, 110–115 (2008).
10. C.-L. Hsieh, Y. Pu, R. Grange, and D. Psaltis, "Digital phase conjugation of second harmonic radiation emitted by nanoparticles in turbid media," Opt. Express **18**, 12283–12290 (2010).
11. H. Ruan, M. Jang, B. Judkewitz, and C. Yang, "Iterative time-reversed ultrasonically encoded light focusing in backscattering mode," Sci. Rep. **4**, 7156 (2014).
12. X. Xu, H. Liu, and L. V. Wang, "Time-reversed ultrasonically encoded optical focusing into scattering media," Nat. Photonics **5**, 154–157 (2011).
13. Y. M. Wang, B. Judkewitz, C. A. DiMarzio, and C. Yang, "Deep-tissue focal fluorescence imaging with digitally time-reversed ultrasound-encoded light," Nat. Commun. **3**, 928 (2012).
14. B. Judkewitz, Y. M. Wang, R. Horstmeyer, A. Mathy, and C. Yang, "Speckle-scale focusing in the diffusive regime with time reversal of variance-encoded light (TROVE)," Nat. Photonics **7**, 300–305 (2013).
15. E. H. Zhou, H. Ruan, C. Yang, and B. Judkewitz, "Focusing on moving targets through scattering samples," Optica **1**, 227–232 (2014).
16. C. Ma, X. Xu, Y. Liu, and L. V. Wang, "Time-reversed adapted-perturbation (TRAP) optical focusing onto dynamic objects inside scattering media," Nat. Photonics **8**, 931–936 (2014).
17. P. Lai, X. Xu, H. Liu, and L. V. Wang, "Time-reversed ultrasonically encoded optical focusing in biological tissue," J. Biomed. Opt. **17**, 0305061 (2012).
18. P. Lai, Y. Suzuki, X. Xu, and L. V. Wang, "Focused fluorescence excitation with time-reversed ultrasonically encoded light and imaging in thick scattering media," Laser Phys. Lett. **10**, 075604 (2013).
19. C. Ma, X. Xu, and L. V. Wang, "Analog time-reversed ultrasonically encoded light focusing inside scattering media with a 33,000 × optical power gain," Sci. Rep. **5**, 8896 (2015).
20. Y. Liu, P. Lai, C. Ma, X. Xu, A. A. Grabar, and L. V. Wang, "Optical focusing deep inside dynamic scattering media with near-infrared time-reversed ultrasonically encoded (TRUE) light," Nat. Commun. **6**, 5904 (2015).
21. B. Jayet, J.-P. Huignard, and F. Ramaz, "Optical phase conjugation in Nd: YVO₄ for acousto-optic detection in scattering media," Opt. Lett. **38**, 1256–1258 (2013).
22. M. Jang, H. Ruan, I. M. Vellekoop, B. Judkewitz, E. Chung, and C. Yang, "Relation between speckle decorrelation and optical phase conjugation (OPC)-based turbidity suppression through dynamic scattering media: a study on *in vivo* mouse skin," Biomed. Opt. Express **6**, 72–85 (2015).
23. I. Yamaguchi and T. Zhang, "Phase-shifting digital holography," Opt. Lett. **22**, 1268–1270 (1997).
24. M. Liebling, T. Blu, and M. Unser, "Complex-wave retrieval from a single off-axis hologram," J. Opt. Soc. Am. A **21**, 367–377 (2004).
25. D. Akbulut, T. J. Huisman, E. G. van Putten, W. L. Vos, and A. P. Mosk, "Focusing light through random photonic media by binary amplitude modulation," Opt. Express **19**, 4017–4029 (2011).
26. I. M. Vellekoop, "Controlling the propagation of light in disordered scattering media," arXiv:0807.1087 (2008).
27. D. Dudley, W. M. Duncan, and J. Slaughter, "Emerging digital micromirror device (DMD) applications," Proc. SPIE **4985**, 14–25 (2003).
28. G. Volpe, G. Volpe, and S. Gigan, "Brownian motion in a speckle light field: tunable anomalous diffusion and selective optical manipulation," Sci. Rep. **4**, 3936 (2014).
29. J. W. Goodman, *Statistical Optics* (Wiley-Interscience, 2000).
30. M. Nixon, O. Katz, E. Small, Y. Bromberg, A. A. Friesem, Y. Silberberg, and N. Davidson, "Real-time wavefront shaping through scattering media by all-optical feedback," Nat. Photonics **7**, 919–924 (2013).